2001

Corrected Article: Exclusive Electroproduction of φ Mesons at 4.2 GeV [Physical. Rev. C 63, 065205, (2001)]

M. Bektasoglu
Old Dominion University

L. Ciciani
Old Dominion University

G. E. Dodge
Old Dominion University, gdodge@odu.edu

T. A. Forest
Old Dominion University

C. E. Hyde-Wright
Old Dominion University, chyde@odu.edu

See next page for additional authors

Original Publication Citation

Bektasoglu, M., Dodge, G.E., Hyde-Wright, C.E., Kuhn, S.E., Qin, L.M., Weinstein, L.B., et al., The CLAS Collaboration (2001). Corrected article: Exclusive electroproduction of φ mesons at 4.2 GeV [Physical. Rev. C 63, 065205, (2001)]. *Physical Review C, 64*(5), 1-11, Article 059901. https://doi.org/10.1103/PhysRevC.64.059901

EDITORIAL NOTE

In Figs. 4, 10, 12, 13, 15, and 16 of the original article (published 22 May 2001) certain symbols in the legends and elsewhere were incorrectly reproduced during the production process. The entire corrected article is republished here. This article should be cited as K. Lukashin *et al.*, Phys. Rev. C **63**, 065205 (2001); **64**, 059901(E) (2001).

Corrected Article: Exclusive electroproduction of ϕ mesons at 4.2 GeV [Phys. Rev. C 63, 065205 (2001)]

K. Lukashin,[1,2,*] E. S. Smith,[2] G. S. Adams,[28] E. Anciant,[7] M. Anghinolfi,[15] B. Asavapibhop,[20] G. Audit,[7] T. Auger,[7] H. Avakian,[14] J. Ball,[3] S. Barrow,[13] M. Battaglieri,[15] K. Beard,[18] M. Bektasoglu,[25] W. Bertozzi,[21] N. Bianchi,[14] A. Biselli,[28] S. Boiarinov,[17] B. E. Bonner,[29] S. Bouchigny,[2] D. Branford,[11] W. J. Briscoe,[16] W. K. Brooks,[2] V. D. Burkert,[2] J. R. Calarco,[22] D. S. Carman,[24] B. Carnahan,[6] L. Ciciani,[25] R. Clark,[5] P. L. Cole,[32,2] A. Coleman,[34,†] D. Cords,[2] P. Corvisiero,[15] D. Crabb,[33] H. Crannell,[6] J. Cummings,[28] P. V. Degtiarenko,[2] L. C. Dennis,[13] E. De Sanctis,[14] R. DeVita,[15] K. S. Dhuga,[16] C. Djalali,[31] G. E. Dodge,[25] J. Domingo,[2] D. Doughty,[8,2] P. Dragovitsch,[13] S. Dytman,[27] M. Eckhause,[34] H. Egiyan,[34] K. S. Egiyan,[35] L. Elouadrhiri,[8,2] A. Empl,[28] R. Fatemi,[33] R. J. Feuerbach,[5] J. Ficenec,[1] K. Fissum,[21] T. A. Forest,[25] A. Freyberger,[2] H. Funsten,[34] S. Gaff,[10] M. Gai,[9] G. Gavalian,[35,‡] S. Gilad,[21] G. Gilfoyle,[30] K. Giovanetti,[18] P. Girard,[31] K. A. Griffioen,[34] M. Guidal,[26] M. Guillo,[31] V. Gyurjyan,[2] J. Hardie,[8,2] D. Heddle,[8,2] F. W. Hersman,[22] K. Hicks,[24] R. S. Hicks,[20] M. Holtrop,[22] J. Hu,[28] C. E. Hyde-Wright,[25] M. M. Ito,[2] D. Jenkins,[1] K. Joo,[33,§] J. Kelley,[10] M. Khandaker,[23] K. Kim,[19] K. Y. Kim,[27] W. Kim,[19] A. Klein,[25] F. J. Klein,[2,‖] M. Klusman,[28] M. Kossov,[17] L. H. Kramer,[12,2] S. E. Kuhn,[25] J. M. Laget,[7] D. Lawrence,[20] A. Longhi,[6] J. J. Manak,[2,¶] C. Marchand,[7] S. McAleer,[13] J. McCarthy,[33] J. W. C. McNabb,[5] B. A. Mecking,[2] M. D. Mestayer,[2] C. A. Meyer,[5] K. Mikhailov,[17] R. Minehart,[33] M. Mirazita,[14] R. Miskimen,[20] V. Muccifora,[14] J. Mueller,[27] G. S. Mutchler,[29] J. Napolitano,[28] S. Nelson,[10] G. Niculescu,[24] I. Niculescu,[16] B. B. Niczyporuk,[2] R. A. Niyazov,[25] A. Opper,[24] G. O'Rielly,[16] J. T. O'Brien,[6] K. Park,[19] K. Paschke,[5] E. Pasyuk,[3] G. A. Peterson,[20] S. Philips,[16] N. Pivnyuk,[17] D. Pocanic,[33] O. Pogorelko,[17] E. Polli,[14] S. Pozdniakov,[17] B. M. Preedom,[31] J. W. Price,[4] L. M. Qin,[25] B. A. Raue,[12,2] A. R. Reolon,[14] G. Riccardi,[13] G. Ricco,[15] M. Ripani,[15] B. G. Ritchie,[3] F. Ronchetti,[14] P. Rossi,[14] D. Rowntree,[21] P. D. Rubin,[30] F. Sabatié,[25] K. Sabourov,[10] C. W. Salgado,[23,2] V. Sapunenko,[15] R. A. Schumacher,[5] V. Serov,[17] Y. G. Sharabian,[35,§] J. Shaw,[20] S. Simionatto,[16] A. Skabelin,[21] L. C. Smith,[33] D. I. Sober,[6] A. Stavinsky,[17] S. Stepanyan,[35] P. Stoler,[28] I. I. Strakovsky,[16] M. Taiuti,[15] S. Taylor,[29] D. Tedeschi,[31,2] R. Thompson,[27] M. F. Vineyard,[30] A. Vlassov,[17] K. Wang,[33] H. Weller,[10] L. B. Weinstein,[25] R. Welsh,[34] D. P. Weygand,[2] S. Whisnant,[31] E. Wolin,[2] L. Yanik,[16] A. Yegneswaran,[2] J. Yun,[25] J. Zhao,[21] B. Zhang,[21] and Z. Zhou[21,**]

(The CLAS Collaboration)

[1]*Department of Physics, Virginia Polytechnic Institute and State University, Blacksburg, Virginia 24061*

[2]*Thomas Jefferson National Accelerator Facility, Newport News, Virginia 23606*

[3]*Department of Physics and Astronomy, Arizona State University, Tempe, Arizona 85287*

[4]*Department of Physics and Astronomy, University of California at Los Angeles, Los Angeles, California 90095*

[5]*Department of Physics, Carnegie Mellon University, Pittsburgh, Pennsylvania 15213*

[6]*Department of Physics, Catholic University of America, Washington, D.C. 20064*

[7]*CEA Saclay, DAPNIA-SPhN, F-91191 Gif-sur-Yvette Cedex, France*

[8]*Christopher Newport University, Newport News, Virginia 23606*

[9]*Physics Department, University of Connecticut, Storrs, Connecticut 06269*

[10]*Physics Department, Duke University, Durham, North Carolina 27706*

[11]*Department of Physics and Astronomy, Edinburgh University, Edinburgh EH9 3JZ, United Kingdom*

[12]*Department of Physics, Florida International University, Miami, Florida 33199*

[13]*Department of Physics, Florida State University, Tallahassee, Florida 32306*

[14]*Istituto Nazionale di Fisica Nucleare, Laboratori Nazionali di Frascati, C.P. 13, I-00044 Frascati, Italy*

[15]*Istituto Nazionale di Fisica Nucleare, Sezione di Genova e Dipartimento di Fisica dell'Universita, I-16146 Genova, Italy*

[16]*Department of Physics, The George Washington University, Washington, D.C. 20052*

[17]*Institute of Theoretical and Experimental Physics, Moscow RU-117259, Russia*

[18]*Department of Physics, James Madison University, Harrisonburg, Virginia 22807*

[19]*Department of Physics, Kyungpook National University, Taegu 702-701, South Korea*

[20]*Department of Physics, University of Massachusetts, Amherst, Massachusetts 01003*

[21]*Massachusetts Institute of Technology–Bates Linear Accelerator, Middleton, Massachusetts 01949*

[22]*Department of Physics, University of New Hampshire, Durham, New Hampshire 03824*

[23]*Norfolk State University, Norfolk, Virginia 23504*

[24]*Department of Physics, Ohio University, Athens, Ohio 45701*
[25]*Department of Physics, Old Dominion University, Norfolk, Virginia 23529*
[26]*Institut de Physique Nucleaire d'Orsay, IN2P3, Boite Postale 1, F-91406 Orsay, France*
[27]*Department of Physics, University of Pittsburgh, Pittsburgh, Pennsylvania 15260*
[28]*Department of Physics, Rensselaer Polytechnic Institute, Troy, New York 12181*
[29]*T.W. Bonner Nuclear Laboratory, Rice University, Houston, Texas 77005-1892*
[30]*Department of Physics, University of Richmond, Richmond, Virginia 23173*
[31]*Department of Physics, University of South Carolina, Columbia, South Carolina 29208*
[32]*Department of Physics, University of Texas, El Paso, Texas 79968*
[33]*Department of Physics, University of Virginia, Charlottesville, Virginia 22903*
[34]*Department of Physics, College of William and Mary, Williamsburg, Virginia 23185*
[35]*Yerevan Physics Institute, 375036 Yerevan, Armenia*
(Received 18 January 2001; published 23 October 2001)

We studied the exclusive reaction $ep \to e'p'\phi$ using the $\phi \to K^+K^-$ decay mode. The data were collected using a 4.2 GeV incident electron beam and the CEBAF Large Acceptance Spectrometer (CLAS) at the Thomas Jefferson National Accelerator Facility. Our experiment covers the range in Q^2 from 0.7 to 2.2 GeV^2, and W from 2.0 to 2.6 GeV. Taken together with all previous data, we find a consistent picture of ϕ production on the proton. Our measurement shows the expected decrease of the t slope with the vector-meson formation time $c\Delta\tau$ below 2 fm. At $\langle c\Delta\tau\rangle = 0.6$ fm, we measure $b_\phi = 2.27 \pm 0.42$ GeV^{-2}. The cross section dependence on W as $W^{0.2\pm0.1}$ at $Q^2 = 1.3$ GeV^2 was determined by comparison with ϕ production at HERA after correcting for threshold effects. This is the same dependence as observed in photoproduction.

DOI: 10.1103/PhysRevC.64.0499XX PACS number(s): 13.60.Le, 12.40.Vv, 14.40.Cs, 25.30.Rw, 99.10.+g

I. INTRODUCTION

Vector-meson photo- and electroproduction have been important tools used to understand the hadronic properties of the photon [1]. For low values of the four-momentum transfer squared, the photon interacts with the target predominantly through vector-meson intermediate states that diffractively scatter off the target. This process, shown in Fig. 1(a), was originally described within the framework of the vector-meson Dominance (VMD) model. The production of the ϕ meson through this mechanism may be interpreted in terms of the hadronic structure of the photon that couples to a virtual meson with a strength proportional to the square of the charge of its constituent quarks. Due to the dominant $s\bar{s}$ quark component in the ϕ meson, quark-exchange (e.g., meson-exchange) mechanisms, and s-channel resonance production are strongly suppressed [2–5]. As a consequence, ϕp scattering at low four-momentum transfer proceeds primarily through pomeron exchange, similar to hadron-hadron diffractive scattering.

It is generally believed that the underlying mechanism for pomeron exchange is multigluon exchange, where the simplest possibility requires at least two gluons since all hadrons are color singlets. A simplification to these calculations was introduced by Donnachie and Landshoff [6,7], who proposed a model whereby the pomeron couples to quarks inside the interacting hadrons as shown in Fig. 1(b). Calculations within this context have been applied to ϕ electroproduction to study the quark substructure of mesons [8,9] and to photoproduction at large momentum transfer [10,11]. In these models the cross section increases slowly with center-of-mass energy, W, reflecting the pomeron trajectory.

At high Q^2 the pomeron can be resolved into two-gluon exchange, and predictions for hard diffractive electroproduction of vector mesons can be made within the context of perturbative QCD [12]. At lower energies ($W \lesssim 10$ GeV), quark-exchange mechanisms [13,14] become significant for the production of vector mesons with valence u and d quarks, but play a limited role in the production of ϕ mesons.

The hadronic structure of the photon arises from fluctuations of the virtual photon into short-lived quark-antiquark ($q\bar{q}$) states of mass M_V during a formation time [1]

$$\Delta\tau = \frac{2\nu}{(Q^2 + M_V^2)}, \tag{1}$$

where $-Q^2$ is the squared mass and ν is the laboratory-frame energy of the virtual photon (see Appendix A for notation). The effect of the formation time on the propagation of these virtual quantum states in strongly interacting media has been observed for ρ mesons propagating inside a proton [15] and inside nuclear targets [16]. To date, no clear depen-

*Present address: Department of Physics, Catholic University of America, Washington, D.C. 20064.
†Present address: Systems Planning and Analysis, 2000 North Beauregard Street, Suite 400, Alexandria, VA 22311.
‡Present address: Department of Physics, University of New Hampshire, Durham, NH 03824.
§Present address: Thomas Jefferson National Accelerator Facility, Newport News, VA 23606.
‖Present address: Department of Physics, Florida International University, Miami, FL 33199.
¶Present address: The Motley Fool, Alexandria, VA 22314.
**Present address: Department of Physics, Computer Science and Engineering, Christopher Newport University, Newport News, VA 23606.

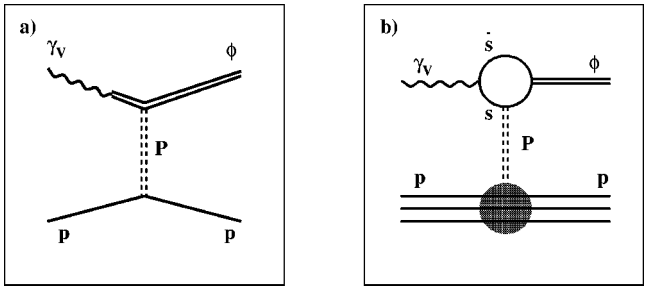

FIG. 1. Representation of ϕ production by (a) the VMD model and (b) the Donnachie and Landshoff pomeron-exchange model.

dence on the formation time has been observed in ϕ meson production by virtual photons [15,17,18].

This paper presents measurements of exclusive ϕ meson electroproduction off a proton target for $2.0 \leqslant W \leqslant 2.6$ GeV and $0.7 \leqslant Q^2 \leqslant 2.2$ GeV^2 where there is extremely limited data. In this kinematic regime, the short formation distance[1] of the virtual $q\bar{q}$ state ($0.35 \leqslant c\Delta\tau \leqslant 0.75$ fm) limits the time for interaction and probes the ϕ production mechanism at small formation times.

In Sec. II we present the details of our experimental techniques and data analysis. It concludes with values for the measured t slopes and total cross sections. In Sec. III we compare our results with previous data, and compare with a geometrical model of the relation between formation time and t slope. The model is discussed in some detail in Appendix B.

II. EXPERIMENT

The experiment was performed using the CEBAF Large Acceptance Spectrometer (CLAS) [19,20] in Hall B of the Thomas Jefferson National Accelerator Facility. The data were taken with a 4.2 GeV electron beam incident on a 5.0 cm liquid hydrogen target in March and April of 1999. The CLAS torus magnet current was set to 2250 A, bending negatively charged particles toward the beam axis. The trigger required a single scattered electron signal, identified as a coincidence of the forward electromagnetic calorimeter (EC) [21] and Cerenkov counters [22]. Data were recorded at an instantaneous luminosity of 0.6×10^{34} cm^{-2} s^{-1} and a typical live time of 95%. This data set has a live-time corrected integrated luminosity $L_{int} = 1.49 \times 10^{39}$ cm^{-2}.

A. Data reduction

In order to reduce the data sample to a manageable size, the data of interest were first preselected using very loose requirements on particle identification, missing mass, and the requirement for W to be above 1.8 GeV. The ϕ mesons were identified through their K^+K^- decay mode. Because of the small acceptance of K^- due to the CLAS magnetic field setting, we required only three final-state particles to be detected: electron, proton, and K^+. The K^- was reconstructed by identification in the $epK^+(X)$ missing mass. The momenta of charged tracks were reconstructed from their curvature in the CLAS magnetic field using a system of drift chambers [23]. The data reduction process selected about 82 000 events for further analysis. The size of this filtered data sample was compact ($\approx$0.5 Gbyte) and easily manageable in comparison with the size of the entire data set ($\approx$1 Tbyte).

[1]In the literature the formation distance is also referred to as coherence length.

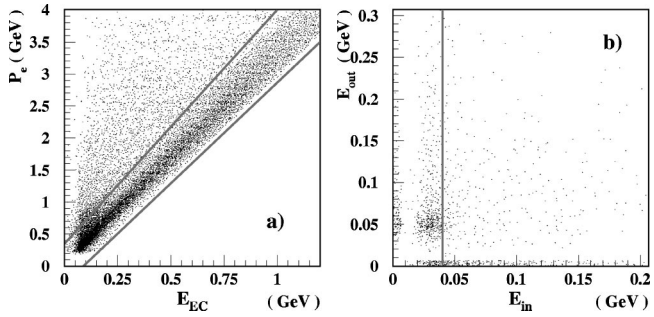

FIG. 2. (a) Electron momentum versus total deposited energy in EC. The solid lines show the applied cuts. (b) Energy deposited by the TOF-identified π^-'s in the outer EC layers versus energy deposited in the inner EC layers. The solid line shows the applied cut $E_{in} > 0.04$ GeV, which retains all good electron candidates.

B. Electron identification

In addition to a fiducial requirement that an electron hit be at least 10 cm from the outer edge of the electromagnetic calorimeter, cuts on energy deposition in the EC were applied in order to avoid misidentification of π^- as e^-. The total energy deposited by an electron in the EC is proportional to the momentum determined by magnetic analysis. This dependence is illustrated in Fig. 2(a). The electron band with the width of the EC resolution is clearly seen. In order to cut out the hadronic background, we applied cuts around this band [the solid lines in Fig. 2(a)]. An additional improvement in e^-/π^- separation was achieved by cutting out the π^- signal based on the energy deposited in the inner

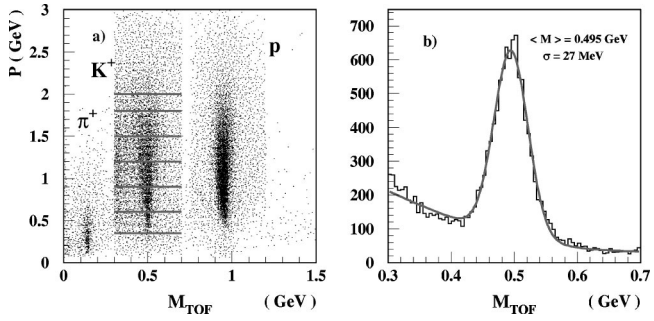

FIG. 3. (a) Positively charged particle momentum versus reconstructed mass for the preselected event sample. The apparent separation between kaons, pions, and protons at high momenta is due to the data preselection cuts. The horizontal lines show the binning in kaon momenta; (b) K^+ reconstructed mass distribution in the momentum bin from 0.9 to 1.2 GeV. The background is due to pion misidentification.

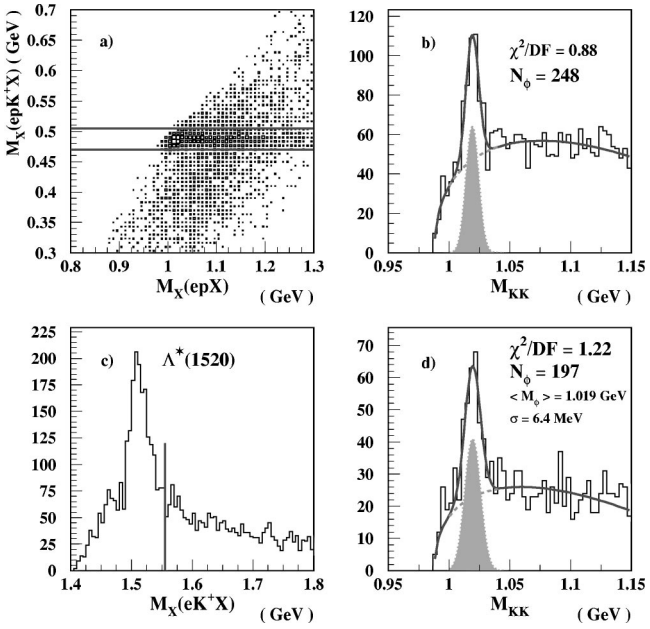

FIG. 4. The ϕ channel separation technique. (a) epK^+X missing mass versus epX missing mass. The horizontal lines show the selection of K^-. (b) M_{KK} mass spectrum of epK^+K^- events. (c) eK^+X missing mass distribution. The line shows the $\Lambda(1520)$ cut. (d) M_{KK} mass distribution with the $\Lambda(1520)$ cut applied.

layer of the calorimeter as shown in Fig. 2(b). The cluster of entries to the left of the line is the π^- signal in the EC. The solid line is the applied cut ($E_{in}>0.04$ GeV) to eliminate pions. To determine this cut we used π^- identified by the time-of-flight (TOF) system of the CLAS [24].

C. Hadron identification

The identification of charged hadrons is illustrated in Fig. 3. The distribution of positively charged particle momenta versus reconstructed mass is shown in Fig. 3(a). Proton, kaon, and positive pion bands are clearly distinguished. The width of the reconstructed mass increases with momentum. However, there is no systematic dependence after careful timing calibration of the detector [24–26].

D. K^+ identification

In order to optimize the signal-to-background ratio in kaon identification, the kaon momentum range was divided into six bins. In each bin the mass distribution was fitted to a Gaussian with a polynomial background to determine the characteristics of the K^+ peak. An example of this procedure is shown in Figs. 3(a) and 3(b). The horizontal lines in Fig. 3(a) show the momentum bins for K^+ identification, and the fitting result for one of the bins is illustrated in Fig. 3(b). To identify kaons, $\pm 2\sigma$ cuts were applied around the mean value $\langle m_{K^+} \rangle$.

E. Proton identification

The proton signal is very clean and does not have a significant background contribution. For proton identification we applied a simple reconstructed mass cut from 0.8 to 1.1 GeV.

F. K^- identification

We identified the K^- using the missing mass technique. The K^- band is clearly seen in Fig. 4(a). The selection used $\pm 2\sigma$ cuts around the K^- peak. The invariant mass, M_{KK}, of the K^+K^- is computed using the known mass of the kaons, the measured momentum of the K^+, and the missing momentum of the event for the K^-. We note that because the masses are large compared to the momenta of the particles, this quantity has significantly better resolution than the epX missing mass.

G. Identification of the signal

Applying the electron and hadron identification cuts described above, we identified about 3800 events of the epK^+K^- final state. In order to eliminate events caused by false triggers on low energy electrons (e.g., from π^0 Dalitz decays) we also required the energy transfer, $\nu = E_e - E_{e'}$, to be smaller than 3.5 GeV. The selected sample includes ϕ mesons, high mass hyperons, and background events that come from particle misidentification.

The most important features of the final selection are shown in Figs. 4(a)–4(c). In the scatter plot of epK^+X versus epX missing mass [see Fig. 4(a)] the signal of the epK^+K^- final state is clearly distinguished from the rest of the data. The solid lines show the $\pm 2\sigma$ selection cuts in the reconstructed K^- mass. Figure 4(b) shows the M_{KK} mass distribution of the selected final state with a prominent peak due to exciting ϕ particles. To extract the total ϕ yield, we fitted the peak with a Gaussian (the integral is shown as the filled area in the plot) and the background with an empirical phase space function,

$$f(M_{KK}) = A\sqrt{M_{KK}^2 - M_{th}^2} + B(M_{KK}^2 - M_{th}^2), \qquad (2)$$

where the threshold $M_{th} = 0.987$ GeV. The fit gives $N_\phi = 248$, a mean value $\langle M_{KK} \rangle = 1019.1 \pm 0.6$ MeV, and $\sigma = 6.0 \pm 0.6$ MeV, where the width of the peak is dominated by the resolution of CLAS.[2] The ϕ signal-to-background ratio is 0.7 within $\pm 2\sigma$ from the mean value of the ϕ peak.

The primary source of physical background consists of high mass hyperons, $ep \to e'K^+Y^*$, with a subsequent decay $Y^* \to N\bar{K}$. The production and decay amplitudes of these particles are not well known. The main channel is the $\Lambda(1520)$ with a cross section larger than ϕ production. Additional contributions come from $\Lambda(1600)$, $\Lambda(1800)$, $\Lambda(1820)$, $\Sigma(1660)$, and $\Sigma(1750)$, which have large branching ratios for decay into the $N\bar{K}$ channel [27]. These backgrounds were investigated by Monte Carlo methods using exactly the same algorithms as the experimental data in order to optimize selection cuts. In order to minimize the number of $\Lambda(1520)$ in the data sample, we require $M_X(eK^+X)$ to be greater than 1.56 GeV. The cut is shown for the data sample with the solid line in Fig. 4(c).

[2]The mass of the ϕ is 1019.417 ± 0.014 MeV, and the decay width [full width at half maximum (FWHM)] is 4.458 ± 0.032 MeV [27].

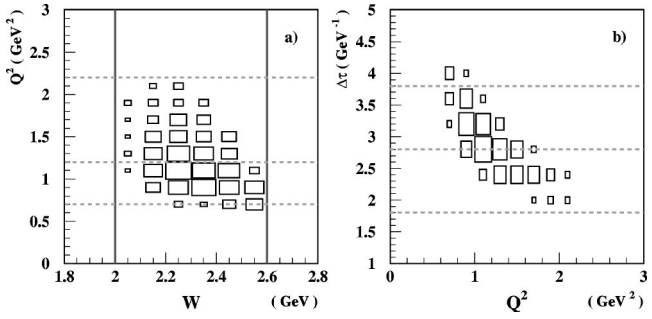

FIG. 5. Kinematic distributions of the selected ϕ events: (a) Q^2 versus W. (b) $\Delta\tau$ versus Q^2. The dashed lines indicate the binning, used later, in Q^2 and $\Delta\tau$; the solid lines show the range of W used in the analysis.

The M_{KK} mass distribution with the $\Lambda(1520)$ cut applied is shown in Fig. 4(d). The simultaneous fit of the ϕ peak and the background gives $N_\phi = 197$, a mean value $\langle M_{KK}\rangle = 1019.4 \pm 0.9$ MeV, and $\sigma = 6.4 \pm 1.1$ MeV. The ϕ signal-to-background ratio is improved and equals 1.3 within $\pm 2\sigma$ of the ϕ peak. The remaining background, consistent with phase space, is due to high-mass hyperon states, nonresonant K^+K^- production and experimental misidentification of a π^+ as a K^+ [events under the K^+ peak in Fig. 3(b)]. We note that the level of the background under the ϕ peak depends on the fitting procedure and will be addressed when we discuss systematic errors.

The kinematic range of the data sample is shown in Fig. 5. The range of Q^2 varies from 0.7 to 2.2 GeV^2, W from 2.0 to 2.6 GeV, and $\Delta\tau$ from 1.8 to 4.0 GeV^{-1} ($c\Delta\tau$ from 0.35 to 0.79 fm). The small values of $c\Delta\tau$ indicate that the formation distance in our kinematic regime is below the hadron size, $2\,r_h \approx 2$ fm. The data binning to calculate the exponential t slope (see below) is indicated in Fig. 5 by horizontal dashed lines, which show the ranges of Q^2 (integrated over $\Delta\tau$) and $\Delta\tau$ (integrated over Q^2). In both cases the data range in W is the same [solid lines in Fig. 5(a)]. We note that finer binning in Q^2 and W is used for the evaluation of the cross sections integrated over t'.

Ideally, with enough statistics and an understanding of the background shape, fits would be used to extract the signal yield in every kinematic bin of interest. With limited statistics this is not possible, and we proceeded by using a side-band subtraction technique.

H. Background subtraction

The side-band technique, as illustrated in Fig. 6, was used to determine the background distribution as a function of Q^2, W, and $-t'$. The signal region was determined within a $\pm 2\sigma$ cut around $\langle M_\phi\rangle$ after excluding the $\Lambda(1520)$ from the final state data sample. The side bands were located $\pm 3\sigma$ away from the ϕ peak, and the number within the band was scaled to the background as determined by the fit [see Fig. 4(d)]. The normalized side-band events were then subtracted in each distribution of interest. This procedure is illustrated in Fig. 6 for the entire data set and was repeated for each kinematic region defined in Table I.

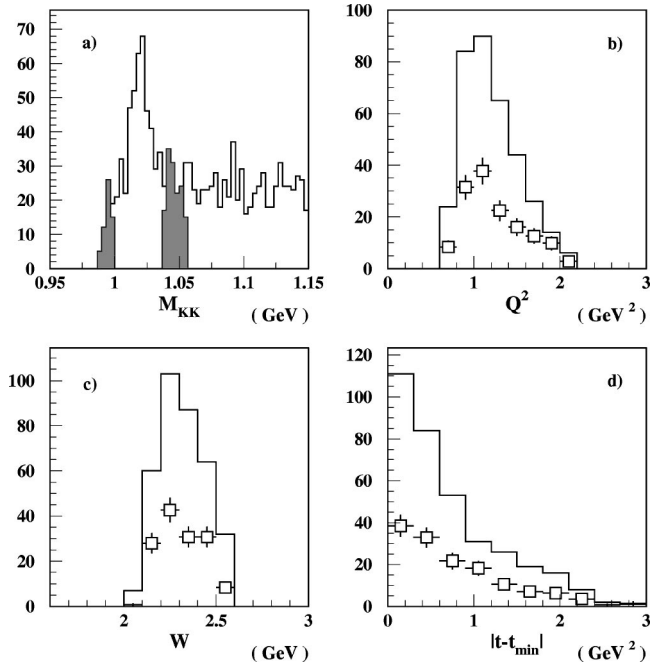

FIG. 6. Side-band background subtraction technique. (a) Location of the side bands; (b), (c), and (d) distributions of events in the signal region (histograms) and in the side bands (open squares) versus Q^2, W, and $|t-t_{min}|$.

I. Acceptance

For the calculation of the acceptance, we used a GEANT-based simulation of CLAS, taking into account trigger efficiency, problematic hardware channels, and the CLAS resolution. The Monte Carlo event sample was generated assuming the VMD model for ϕ electroproduction. Two iterations in the acceptance calculation were made to adjust the VMD parameters to be close to the data. In each kinematic region, the acceptance was calculated from the ratio of reconstructed to generated ϕ events with the same kinematics and particle identification cuts that were applied to the data. Figure 7 shows the acceptance as a function of Q^2 and $-t'$ for the entire data set. This procedure was also used to calculate the acceptance as a function of W and $\Delta\tau$ in each kinematic bin.

J. Radiative corrections

For the calculation of the radiative corrections, we used the peaking approximation [28]. We define the radiative cor-

TABLE I. The measured values of the t-slope parameter, b_ϕ, fitted to the data for $-t' < 1.2$ GeV^2. The errors are statistical only.

Kinematic region	Q^2 and $c\Delta\tau$ range	$\langle Q^2\rangle$ (GeV^2)	$\langle c\Delta\tau\rangle$ (fm)	b_ϕ (GeV^{-2})
All data	0.7–2.2 GeV^2	1.02		2.27 ± 0.42
	0.35–0.75 fm		0.6	
Low Q^2	0.7–1.2 GeV^2	0.87	–	2.31 ± 0.59
High Q^2	1.2–2.2 GeV^2	1.47	–	2.10 ± 0.52
Low $c\Delta\tau$	0.35–0.55 fm	–	0.49	2.04 ± 0.42
High $c\Delta\tau$	0.55–0.75 fm	–	0.63	2.12 ± 0.46

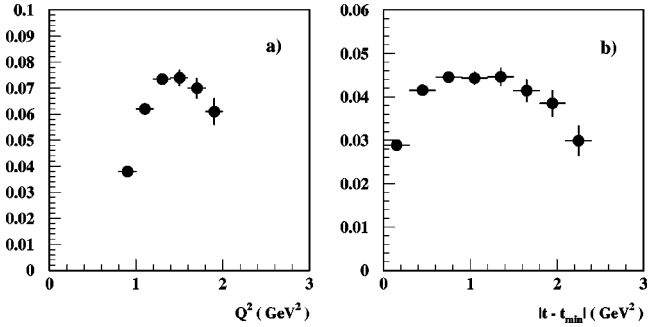

FIG. 7. Acceptance as a function of Q^2 and $-t'$.

rections in each bin of every kinematic variable as the ratio $F^{rad}=N_{norad}/N_{rad}$, where N_{rad} and N_{norad} are the generated ϕ yields with radiative effects turned on and off, respectively. The model for the ϕ production cross section employed for the computation of acceptance was also used for the studies of radiative corrections. The ratios were calculated with the same kinematics and particle identification cuts that were applied to the data. The simulated ϕ mass distributions with and without radiative effects are shown in Fig. 8(a). The inverse radiative correction factor, $1/F^{rad}$, as a function of Q^2 is shown in Fig. 8(b). The correction factors as a function of $-t'$ in all four kinematic regions are of the order of 1.4 and uniform over the kinematics considered here.

K. Data normalization

The final step in the analysis procedure was the normalization of the ϕ yield to the integrated luminosity, the virtual photon flux, and all calculated corrections as

$$\sigma(Q^2,W)=\frac{N_\phi/B_{\phi\to K^+K^-}}{\Delta Q^2\Delta W}\frac{F^{acc}F^{rad}F^{win}}{2\pi\Gamma(Q^2,W)L_{int}}, \qquad (3)$$

where ΔQ^2 and ΔW are the bin widths in Q^2 and W, $\Gamma(Q^2,W)$ is the virtual photon flux, L_{int} is the integrated luminosity, N_ϕ is the ϕ yield in the bin, F^{acc} is the acceptance factor in a given bin, F^{win} is a small correction factor for production from the target windows ($\approx 1\%$), F^{rad} is the radiative correction factor, and $B=0.492\pm 0.007$ is the decay

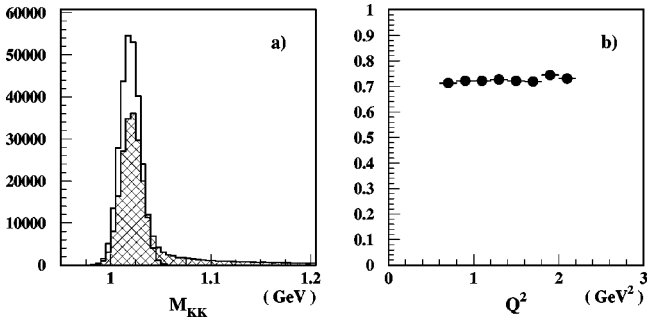

FIG. 8. Simulated data: (a) ϕ peak, convoluted with the measured CLAS resolution, with radiative effects turned off (solid) and turned on (hatched histogram). (b) Inverse radiative correction factor, $1/F^{rad}$, as a function of Q^2.

TABLE II. The averaged values of W, ϵ, $\Gamma(Q^2,W)$, and $\sigma(Q^2,W)$ as a function of Q^2. The numbers given for the virtual photon flux, $\Gamma(Q^2,W)$, computed event by event, are the mean and the standard deviation for the bin.

Q^2 bin (GeV^2)	$\langle W\rangle$ (GeV)	$\langle\epsilon\rangle$	$\Gamma(Q^2,W)$ (10^{-4} GeV^{-3})	$\sigma(Q^2,W)$ (nb)
0.8–1.0	2.37	0.51	1.50 ± 0.15	27.6 ± 6.1
1.0–1.2	2.31	0.50	1.12 ± 0.10	24.2 ± 5.4
1.2–1.4	2.28	0.49	0.879 ± 0.067	23.0 ± 5.2
1.4–1.6	2.28	0.44	0.701 ± 0.050	20.8 ± 5.7
1.6–1.8	2.25	0.42	0.562 ± 0.033	14.5 ± 6.4

branching ratio for $\phi\to K^+K^-$ [27]. The virtual photon flux was calculated on an event-by-event basis and averaged for each kinematic bin as

$$\Gamma(Q^2,W)=\frac{\alpha}{8\pi^2}\frac{W}{M_pE_e^2}\frac{W^2-M_p^2}{M_pQ^2}\frac{1}{1-\epsilon}, \qquad (4)$$

where M_p is the mass of the proton, E_e is the electron beam energy, and ϵ is the polarization of the virtual photon:

$$\epsilon=\frac{4E_e(E_e-\nu)-Q^2}{4E_e(E_e-\nu)+2\nu^2+Q^2}. \qquad (5)$$

L. Cross section, $\sigma(Q^2,W)$

The cross section integrated over all t', $\sigma(Q^2,W)$, was extracted in five bins over a Q^2 range from 0.8 to 1.8 GeV^2 with a bin width of 0.2 GeV^2. The range in W was determined as the allowed kinematic range for each Q^2. The binning, values of the virtual photon flux used during normalization, $\Gamma(Q^2,W)$, and the measured cross section are given in Table II. The table shows statistical errors only.

M. Differential cross section, $d\sigma/dt'$

The measured cross section, $d\sigma/dt'$, is generally parametrized at small $-t'$ by

$$\frac{d\sigma}{dt'}=A_\phi e^{b_\phi t'}. \qquad (6)$$

The entire t' range ($0\leqslant -t'\leqslant 2.6$ GeV^2) can be fitted to a single exponential with a slope $b_\phi=1.61\pm 0.31$ GeV^{-2} and a $\chi^2=0.9$/DF. However, Eq. (6) is only expected to be valid at small $-t'$, so we have restricted our analysis to $-t'$ less than 1.2 GeV^2, which also allows direct comparison to previous measurements. For this restricted range, we obtain $b_\phi=2.27\pm 0.42$ GeV^{-2} (solid line in Fig. 9). We also performed fits in the four overlapping kinematic regions specified in Table I: two ranges in Q^2 (integrated over $c\Delta\tau$) and two ranges in $c\Delta\tau$ (integrated over Q^2). The results of these fits are given in Table I.

We note that at larger $-t'$, there is an apparent change in the slope of the distribution with a break at $-t'\approx 1.3$ GeV^2. This suggests that additional mechanisms may be present at

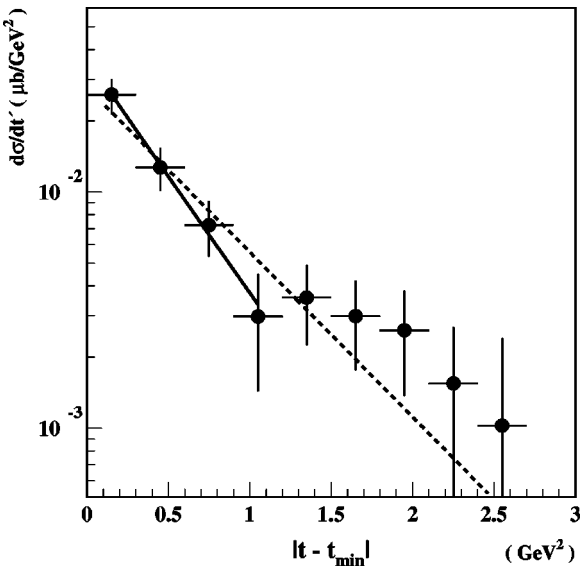

FIG. 9. The $d\sigma/dt'$ differential cross section for exclusive ϕ electroproduction off the proton with fits to the entire $-t'$ range (dashed) and $-t'$ less than 1.2 GeV^2 (solid).

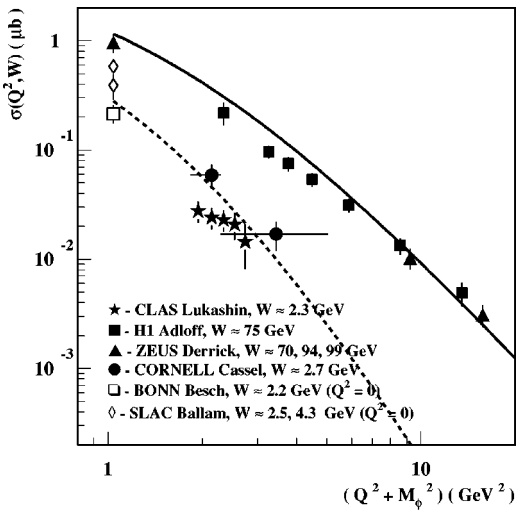

FIG. 10. The ϕ meson cross section dependence on Q^2 for photo- and electroproduction. Electroproduction data H1 Collaboration (Adloff *et al.*) are from Ref. [34], ZEUS Collaboration (Derrick *et al.*) from Refs. [35,36], and Cornell (Cassel *et al.*) from Ref. [15]. Photoproduction data Bonn (Besch *et al.*) are from Ref. [37], and SLAC (Ballam *et al.*) from Ref. [38]. The solid and dashed curves are the pomeron-exchange model predictions for $W=70$ GeV and for $2.0<W<2.6$ GeV, respectively [10].

$-t' \geqslant 1$ GeV^2. Despite the fact that the break is not statistically significant, we discuss possible mechanisms for a slope change. A similar pattern is observed in hadron-hadron elastic scattering [29,30], where a dip is observed at $-t \approx 1.4$ GeV^2 followed by a second maximum at $-t \approx 1.8$ GeV^2. However, ϕ photoproduction data do not show a change in the slope for $-t \leqslant 2$ GeV^2 [11]. *s*-channel production of resonances results in a large measured value of $-t'$. However, there are no known resonances that decay into ϕN. Finally, imperfect background subtraction could also lead to an enhancement at large $-t'$, but should be subsumed into our quoted systematic errors.

N. Systematic errors

Estimates of our systematic errors for the cross section, $\Delta\sigma$, and the *t*-slope parameter, Δb_ϕ, are given in Table III. The errors are averaged over the kinematics of the experiment, although the lowest Q^2 cross section point may have about twice this systematic uncertainty due to the steepness of the acceptance function [see Fig. 7(a)]. To estimate the systematic errors due to background subtraction, a complete analysis of the cross section and *t*-slope parameter was performed using two different assumptions for the shape of the background: phase space and a constant. The difference between these results is quoted as the systematic error due to background subtraction. The systematic errors due to acceptance and radiative corrections are discussed in Refs. [31] and [32], respectively. Additional details can be found in Ref. [25]. We note that the overall uncertainty is dominated by statistical errors.

TABLE III. Summary of the contributions to the systematic errors.

Source	$\Delta\sigma$(%)	Δb_ϕ(%)
Target stability	0.7	–
Target walls	1.0	–
Acceptance	7.8	5.0
Radiative corrections	4.7	–
Background subtraction	5.4	4.6
Total	10.7	6.8

III. RESULTS

A. Cross section dependence on Q^2 and W

The world data on elastic virtual photon production of ϕ mesons are shown as a function of Q^2 in Fig. 10, and as a function of W in Fig. 11. Selected photoproduction data are also plotted for completeness.[3] We show the data on both plots with common symbols.

All HERA data [34–36] correspond to W ranging from 40 to 130 GeV, where the gluonic density in the proton at low $x = Q^2/2M_p\nu$ plays a significant role. Only the Cornell measurement [15] exists at low W, corresponding to x in the valence region.[4] For the high-energy data, the Q^2 behavior of the cross section is well described by the vector-meson propagator squared. The data are not yet in the asymptotic perturbative QCD regime where the longitudinal cross section for vector-meson production is dominant, and should scale as Q^{-6} [39]. Nevertheless, the longitudinal contribu-

[3]Additional data of ϕ production on nuclear targets [33] are available at $\langle W \rangle \approx 14$ GeV.

[4]We note that data points from Ref. [15] have different integration ranges for the cross section as a function of Q^2 and W presented in Figs. 10 and 11.

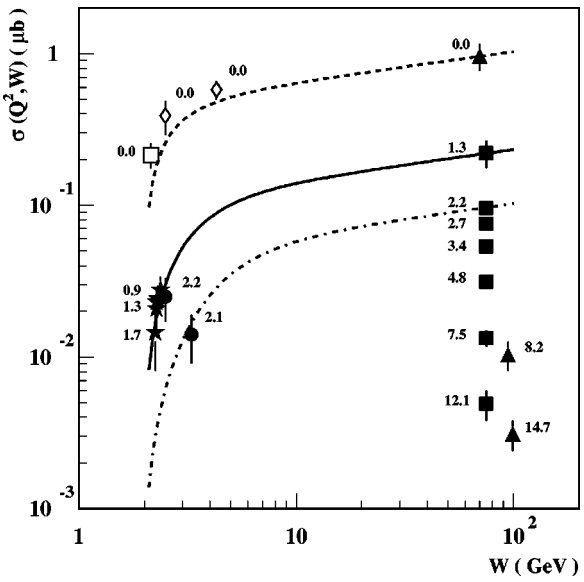

FIG. 11. The ϕ meson cross section dependence on W for photo- and electroproduction. The Q^2 values of the measurements are printed near the corresponding data points. All data points are from the same references as in Fig. 10. The curves, described in the text, correspond to a Q^2 of 0, 1.3, and 2.2 GeV^2.

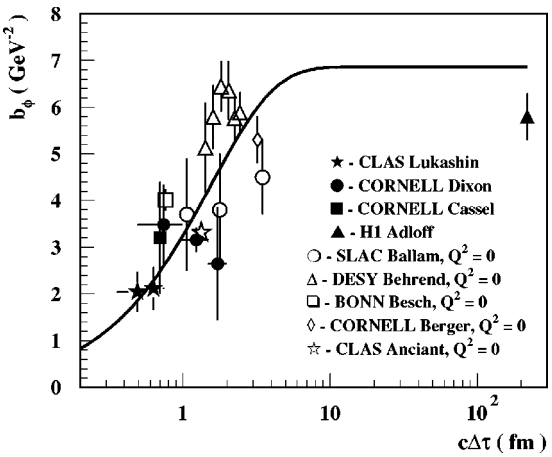

FIG. 12. The dependence of the t slope, b_ϕ, on $c\Delta\tau$. The electroproduction data Cornell (Dixon *et al.*) are from Refs. [17,18], Cornell (Cassel *et al.*) from Ref. [15], and H1 Collaboration (Adloff *et al.*) from Ref. [34]. The photoproduction data Bonn Collaboration (Besch *et al.*) are from Ref. [37], SLAC (Ballam *et al.*) from Ref. [38], DESY (Behrend *et al.*) from Ref. [42], and CLAS Collaboration (Anciant *et al.*) from Ref. [11].

tion becomes increasingly important and must be treated systematically. For example, ρ mesons in muoproduction at large Q^2 are found to be dominantly in the helicity zero spin state [40].

Pomeron-exchange models, such as those described in the introduction, reproduce the Q^{-4} behavior of the data at large Q^2. The predictions of a model [10], based on the Donnachie-Landshoff pomeron exchange [Fig. 1(b)], are shown in Fig. 10 for the W range of our experiment ($2.0 < W < 2.6$ GeV) and at $W = 70$ GeV. The model describes the data reasonably well at high W and reproduces the trend at low W but overestimates the new cross section results presented here. We note that our data are close to the ϕ production threshold, where the cross section increases rapidly as a function of center-of-mass energy. In the model of Pichowsky and Lee [8], the transition from a cross section that slowly decreases with Q^2 to one that falls off as Q^{-4} occurs at a threshold that increases with the current-quark mass of the vector meson. No clear threshold is visible in the ϕ data, but the scarcity of points precludes drawing conclusions.

The photoproduction cross section increases slowly with W, reflecting the pomeron trajectory. At higher Q^2, a stronger dependence on W has been observed in preliminary analysis of HERA data [41]. If the cross section is parametrized as W^δ, δ varies from about 0.2 for photoproduction to $\delta \sim 0.7$ at a Q^2 of 8 GeV^2. This increased dependence of the cross section on W has been interpreted as being due to the rise of the gluon momentum density in the proton at small x [39].

To be able to extract the W dependence by comparing our measurement at $Q^2 = 1.3$ GeV^2 to HERA data at the same Q^2 and $\langle W \rangle = 75$ GeV, threshold effects must be taken into account. For example, threshold behavior can be clearly seen in the photoproduction data [42] (see Fig. 11). The reduced phase space near threshold behaves as $(\vec{p}_\phi/\vec{q})^2$, where $\vec{p}_\phi$ and $\vec{q}$ are the center-of-mass three-momenta of the ϕ and virtual photon, respectively. This dependence of the cross section on W can be parametrized as

$$\sigma(W) = \sigma_0 \left(\frac{\vec{p}_\phi}{\vec{q}} \right)^2 \left(\frac{W}{W_0} \right)^\delta . \tag{7}$$

Correcting for the threshold factor, our measurement of the cross section becomes $\sigma_{corr}(Q^2 = 1.3) = 110 \pm 27$ nb, and using the HERA measurement, $\sigma(Q^2 = 1.3) = 220 \pm 51$ nb [34], we obtain $\delta = 0.2 \pm 0.1$. The quoted uncertainties were obtained by summing the statistical and systematic errors in quadrature. This slope is consistent with that measured in photoproduction. The curves of $\sigma(W)$ are shown in Fig. 11 for Q^2 of 0, 1.3, and 2.2 GeV^2 and $\delta = 0.2$. The curves are normalized to the HERA data (σ_0, W_0) that are far from the production threshold.

B. Dependence of the t slope on $c\Delta\tau$

The dependence of the t slope, b_ϕ, on formation distance, $c\Delta\tau$, for ϕ meson production is shown in Fig. 12 together with previous data. In the terminology of the uncertainty principle, $\Delta\tau$ is the time during which the virtual photon, with mass $\sqrt{Q^2}$, can fluctuate into a ϕ meson [1]. We expect that b_ϕ should decrease at low $\Delta\tau$ as the interaction becomes more pointlike. The previous electroproduction measurements [15,17,18] do not show the expected behavior. However, a consistent picture emerges when we include photoproduction data as well. Both of our data points (solid stars) lie in the region of $c\Delta\tau$ below 1 fm and show a decrease of b_ϕ with decreasing formation time when combined with other data. This is consistent with the well-measured dependence for ρ meson production [15] as discussed in Appendix

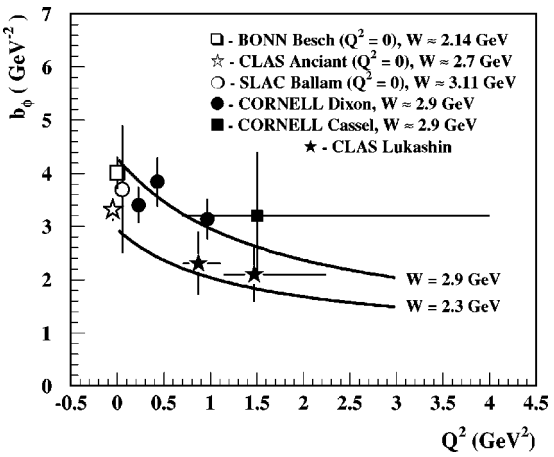

FIG. 13. The dependence of the t slope, b_ϕ, on Q^2. Photoproduction data Bonn (Besch *et al.*) are from Ref. [37], SLAC (Ballam *et al.*) from Ref. [38], and CLAS Collaboration (Anciant *et al.*) from Ref. [11]. Electroproduction data Cornell (Dixon *et al.*) are from Refs. [17,18] and Cornell (Cassel *et al.*) from Ref. [15].

B. To fit the ϕ meson data to Eq. (B5), we constrain the parameter r_h to the value extracted from the fit to the ρ data [Eq. (B6)]. This yields

$$b_\phi(c\Delta\tau)=(6.87\pm0.17)[1-e^{-c\Delta\tau/2(0.78)}] \tag{8}$$

with $\chi^2/\mathrm{DF}=4.8$. The fit to the ϕ data is shown in Fig. 12 with the solid curve. The ratio of b_ϕ/b_ρ indicates that the ϕ meson interaction size, R_ϕ^{int}, is smaller than that for the ρ meson:

$$\frac{b_\phi}{b_\rho}=\left(\frac{R_\phi^{int}}{R_\rho^{int}}\right)^2=0.87\pm0.08. \tag{9}$$

A summary of the existing measurements of b_ϕ together with our results is shown in Fig. 13. Previous ϕ electroproduction measurements are consistent with no Q^2 or $c\Delta\tau$ dependence [15,18]. We observe a low value of $b_\phi\approx2.2$ GeV^{-2}, which, taken together with the values measured in photoproduction, shows a significant dependence on Q^2. However, the Q^2 dependence of b_ϕ can be explained by the implicit dependence of $c\Delta\tau$ on Q^2 [Eq. (B7)]. This is shown in Fig. 13 where we plot the dependence of b_ϕ on Q^2 using Eq. (8) and the relation in Eq. (B7) at two values of W. The lower curve, at $W=2.3$ GeV, corresponds to our kinematics and connects our measurements with photoproduction values. The upper curve is closer to the Cornell kinematics.

Because the value of $c\Delta\tau$ is smaller than the size of the nucleon, the scattering may be considered to be pointlike. The application of QCD-inspired models, sensitive to the quark structure of the interacting meson and nucleon, should provide an interesting interpretation of the observed $b(\Delta\tau)$ and $b(Q^2)$ dependencies. It has been argued that with increasing Q^2 the radius of the virtual vector meson will shrink [1], and a corresponding decrease of b should be observed. At large enough Q^2, quark models [43,44] predict the decrease of the transverse dimension of the vector meson as $r_V\sim r_h M/\sqrt{M^2+Q^2}$. The mass scale M represents a typical hadronic mass scale, which might be as small as the vector-meson mass, e.g., $M_\phi=1020$ MeV, but is likely to be large compared to the Q^2 values of this experiment. Even though we do not need to invoke an explicit Q^2 dependence to describe our data, we note that the effects of transverse size and fluctuation times are not easily separated, especially when fine binning is prohibitive due to limited statistics.

IV. SUMMARY

The electroproduction of the $\phi(1020)$ vector meson was measured for Q^2 from 0.7 to 2.2 GeV^2, W from 2.0 to 2.6 GeV, and $\Delta\tau$ from 1.8 to 4.0 GeV^{-1} ($c\Delta\tau$ from 0.35 to 0.79 fm). A sample of 197 $\phi(1020)$ mesons was accumulated for the exclusive reaction of $ep\rightarrow e'p'\phi$ with the CLAS detector in Hall B at the Thomas Jefferson National Accelerator Facility.

(i) Taken together with the world data sample, we find a consistent picture of ϕ production on the proton. Yet the scarcity of ϕ data do not permit a precise quantitative description of the production process.

(ii) We observe the expected decrease of the slope b_ϕ of $d\sigma/dt'$ on the formation length $c\Delta\tau$ below 2 fm. The rate of the b_ϕ decrease is similar to that in ρ meson production, but with a lower asymptotic value. Using a simple geometric model, the data show that the interaction size of ϕ mesons with a proton is smaller than for ρ mesons.

(iii) The ϕ production cross section measurement adds new information at low values of Q^2 and W. The cross section dependence on Q^2 is qualitatively reproduced by pomeron-exchange models. The cross section dependence on W as $W^{0.2\pm0.1}$ at $Q^2=1.3$ GeV^2 was determined by comparison to ϕ production at HERA after correcting for threshold effects. This dependence is the same as observed in photoproduction.

Additional electro- and photoproduction data from CLAS are currently being analyzed and will increase the overall qualitative and quantitative understanding of the physics that underlies vector meson production.

ACKNOWLEDGMENTS

We would like to acknowledge the efforts of the Accelerator staff, the Physics Division, and the Hall B technical staff that made this experiment possible. This work was supported in part by the U.S. Department of Energy, including DOE Contract No. DE-AC05-84ER40150, the National Science Foundation, the French Commissariat á l'Energie Atomique, the Italian Istituto Nazionale di Fisica Nucleare, and the Korea Science Engineering Foundation. We would also like to acknowledge useful discussions with D. Cassel, M. Pichowsky, and B. Z. Kopeliovich.

APPENDIX A: NOTATION

We denote the four-momenta of the incident and scattered electron by p_e and $p_{e'}$, the virtual photon by $q\equiv p_e-p_{e'}$, and the target and recoil proton by p_p and $p_{p'}$. Each four-vector can be written as $(E,\vec{p})$ with appropriate subscripts.

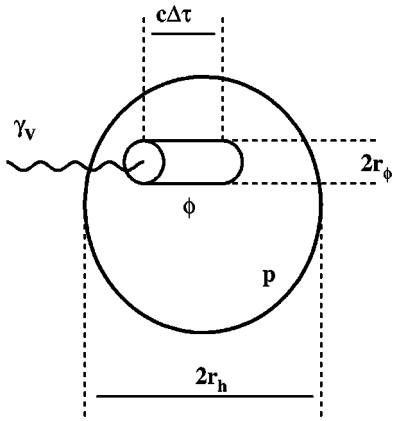

FIG. 14. Space-time picture of the $\gamma_V p$ scattering through the conversion of the virtual photon into the virtual ϕ meson inside the target proton.

We use the common notation for Lorentz invariants: $Q^2=-q^2>0$, $\nu=q\cdot p_p/M_p$ (M_p is the mass of the proton), the squared hadronic center-of-mass energy $W^2=(q+p_p)^2$, and $t=(p_p-p_{p'})^2$ is the four-momentum transfer to the target. The above-threshold momentum transfer is given by $t'=t-t_{min}(Q^2,W)<0$, where $-t_{min}$ is the minimum value of $-t$ for fixed kinematics.

APPENDIX B: GEOMETRIC MODEL

We describe a qualitative picture of vector-meson diffractive scattering within a simple geometric model. A sketch of the process is shown in Fig. 14. The virtual photon is converted into the virtual vector meson (of radius r_V), which diffractively interacts with the proton (of radius r_h) during a formation time $\Delta\tau$. Differential elastic cross sections are closely related to the charge form factors $F(t)$ of colliding hadrons at high energy [29,45]. For small values of t, the form factors are related to the charge radii $\langle r^2\rangle$, via

$$F(t)=1+\frac{1}{6}\langle r^2\rangle t+O(t^2). \tag{B1}$$

For hadron-hadron elastic scattering [29], the cross sections depend exponentially on t:

$$\frac{d\sigma/dt}{(d\sigma/dt)_{t=0}}=e^{bt}. \tag{B2}$$

Comparison of Eqs. (B1) and (B2), and noting that the cross section is proportional to the square of the form factor, lead to a relationship between the radius of interaction, R_V^{int}, and the t-slope parameter b:

$$b=\frac{1}{3}(R_V^{int})^2. \tag{B3}$$

The radius of interaction can be written as

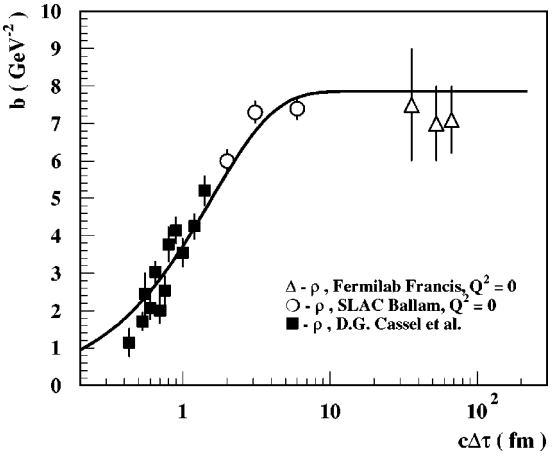

FIG. 15. The t-slope parameter dependence on $c\Delta\tau$ for selected photo- and electroproduction data of ρ mesons. The data show a clear decrease of b with decreasing $c\Delta\tau$ below 2 fm. The curve is a fit to Eq. (B5). The photoproduction data SLAC (Ballam *et al.*) are from Ref. [38] and Fermilab (Francis *et al.*) from Ref. [46]. The electroproduction data Cornell (Cassel *et al.*) are from Ref. [15].

$$(R_V^{int})^2\propto\langle r_h^2\rangle+\langle r_V^2(Q^2)\rangle, \tag{B4}$$

where r_h and r_V are the radii of the nucleon and vector meson, respectively.

Because of the virtuality of the vector meson, the interaction region should also decrease if the formation distance is less than the size of the nucleon ($c\Delta\tau\lesssim 2r_h\approx 2$ fm). A representative sample of the large body of ρ data shown in Fig. 15 suggests the following phenomenological parametrization for the t-slope dependence on $c\Delta\tau$:

$$b(c\Delta\tau)=\frac{1}{3}(1-e^{-c\Delta\tau/2r_h})(R_V^{int})^2. \tag{B5}$$

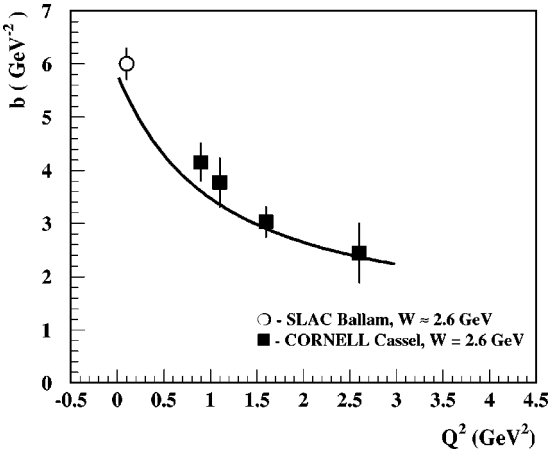

FIG. 16. The t-slope parameter dependence on Q^2 for the photo- and electroproduction of ρ mesons at $W=2.6$ GeV. The data show a clear decrease of b with increasing Q^2. The curve is a fit to Eq. (B5). The photoproduction data SLAC (Ballam *et al.*) are from Ref. [38]. The electroproduction data Cornell (Cassel *et al.*) are from Ref. [15].

A two-parameter fit to Eq. (B5), ignoring any explicit dependence of r_ρ on Q^2, yields

$$b_\rho(c\Delta\tau) = (7.86 \pm 0.26)[1 - e^{-c\Delta\tau/2(0.78\pm0.05)}] \quad \text{(B6)}$$

with $\chi^2/\mathrm{DF} = 2.08$.

However, Eq. (B5) also has an indirect dependence on Q^2 through $c\Delta\tau$. At fixed W, we can write Eq. (1) as

$$c\Delta\tau = \frac{c(W^2 - M_p^2 + Q^2)}{M_p(Q^2 + M_\rho^2)}. \quad \text{(B7)}$$

Thus, we can plot Eq. (B5) as a function of Q^2, using this expression for $c\Delta\tau$. This is shown in Fig. 16 for ρ data at the fixed value of $W = 2.6$ GeV [15]. Thus, we see that most, if not all, of the variation of the slope parameter b can be accounted for by changes in the fluctuation time. For the kinematics of this experiment, $c\Delta\tau$ (≈ 0.5 fm) is small compared to the size of the nucleon, so we expect the fluctuation time factor to be significant for our ϕ data.

[1] T.H. Bauer *et al.*, Rev. Mod. Phys. **50**, 261 (1978).
[2] P.G.O. Freund, Nuovo Cimento A **48**, 541 (1967).
[3] V. Barger and D. Cline, Phys. Rev. Lett. **24**, 1313 (1970).
[4] H. Joos, Phys. Lett. **24B**, 103 (1967).
[5] K. Kajantie and J.S. Trefil, Phys. Lett. **24B**, 106 (1967).
[6] A. Donnachie and P.V. Landshoff, Nucl. Phys. **B244**, 322 (1984).
[7] A. Donnachie and P.V. Landshoff, Phys. Lett. B **185**, 403 (1987).
[8] M.A. Pichowsky and T.-S.H. Lee, Phys. Rev. D **56**, 1644 (1997).
[9] J.-M. Laget, Phys. Rev. Lett. **85**, 4682 (2000).
[10] Calculations based on J.-M. Laget and R. Mendez-Galain, Nucl. Phys. **A581**, 397 (1995).
[11] CLAS Collaboration, E. Anciant *et al.*, Phys. Rev. Lett. **85**, 4682 (2000).
[12] L.L. Frankfurt, G.A. Miller, and M.I. Strikman, Annu. Rev. Nucl. Sci. **44**, 501 (1994).
[13] M. Vanderhaeghen, P.A.M. Guichon, and M. Guidal, Phys. Rev. D **56**, 2982 (1997).
[14] H.W. Wang and P. Kroll, hep-ph/0005318.
[15] D.G. Cassel *et al.*, Phys. Rev. D **24**, 2787 (1981).
[16] HERMES Collaboration, K. Ackerstaff *et al.*, Phys. Rev. Lett. **82**, 3025 (1999).
[17] R. Dixon *et al.*, Phys. Rev. Lett. **39**, 516 (1977).
[18] R. Dixon *et al.*, Phys. Rev. D **19**, 3185 (1979).
[19] W.K. Brooks, Nucl. Phys. **A663-664**, 1077 (2000).
[20] B. Mecking *et al.* (unpublished).
[21] M. Amarian *et al.*, Nucl. Instrum. Methods (submitted).
[22] G. Adams *et al.*, Nucl. Instrum. Methods (submitted).
[23] M.D. Mestayer *et al.*, Nucl. Instrum. Methods Phys. Res. A **449**, 81 (2000).
[24] E.S. Smith *et al.*, Nucl. Instrum. Methods Phys. Res. A **432**, 265 (1999).
[25] K. Loukachine, Ph.D. thesis, Virginia Polytechnic Institute and State University (2000).
[26] S.J. Taylor, Ph.D. thesis, Rice University, 2000.
[27] Particle Data Group, D.E. Groom *et al.*, Eur. Phys. J. C **15**, 1 (2000).
[28] R. Ent *et al.*, Phys. Rev. C (submitted).
[29] K. Goulianos, Phys. Rep. **101**, 169 (1983).
[30] R. Castaldi and G. Sanguinetti, Annu. Rev. Nucl. Part. Sci. **35**, 351 (1985).
[31] T. Auger, Ph.D. thesis, Université de Paris, 1999.
[32] R. Thompson, Ph.D. thesis, University of Pittsburgh, 2000.
[33] M. Arneodo *et al.*, Nucl. Phys. **B429**, 503 (1994).
[34] H1 Collaboration, C. Adloff *et al.*, Phys. Lett. B **483**, 360 (2000).
[35] ZEUS Collaboration, M. Derrick *et al.*, Phys. Lett. B **380**, 220 (1996).
[36] ZEUS Collaboration, M. Derrick *et al.*, Phys. Lett. B **377**, 259 (1996).
[37] H. J. Besch *et al.*, Nucl. Phys. **B70**, 257 (1974).
[38] J. Ballam *et al.*, Phys. Rev. D **5**, 545 (1972); **7**, 3150 (1973).
[39] S.J. Brodsky *et al.*, Phys. Rev. D **50**, 3134 (1994).
[40] EMC Collaboration, J.J. Aubert *et al.*, Phys. Lett. **161B**, 203 (1985).
[41] B. Naroska, hep-ex/0006010.
[42] H.-J. Behrend *et al.*, Nucl. Phys. **B144**, 22 (1978).
[43] L. Frankfurt, W. Koepf, and M. Strikman, Phys. Rev. D **54**, 3194 (1996).
[44] B.Z. Kopeliovich *et al.*, Phys. Lett. B **309**, 179 (1993).
[45] B. Povh, hep-ph/9806379, and references therein.
[46] W. Francis *et al.*, Phys. Rev. Lett. **38**, 633 (1977).